Growth and Aggregation of Vaterite in Seeded-Batch Experiments

Jens-P. Andreassen
Dept. of Chemical Engineering, Norwegian University of Science and Technology, 7491 Trondheim, Norway

M. J. Hounslow
Particle Products Group, Dept. of Chemical and Process Engineering, The University of Sheffield, Sheffield, S10 2TN United Kingdom

DOI 10.1002/aic.10205
Published online in Wiley InterScience (www.interscience.wiley.com).

Seeded-batch crystallization experiments allowing study of the growth and aggregation of the Vaterite modification of calcium carbonate are reported. Results are reported for initial relative supersaturation ($\sigma = S - 1$) values in the range 1.66 to 6.70, stirrer speeds in the range 400 and 1200 rpm, and at temperatures of 25 and 40°C. It is found that in all cases the linear rate of growth of the particles is size independent and depends on relative supersaturation squared. The aggregation process is apparently size independent with a rate constant that is directly proportional to the instantaneous growth rate and decreases with increasing stirrer speed. The behavior of the aggregation rate constant is very well described by the model recently proposed by Liew et al., in which the efficiency of the aggregation process is predicted to depend only on the dimensionless strength of the particles and the nature of the flow field. It is concluded that Vaterite forms aggregates with crystalline bridges having an effective strength of approximately 25% of that of calcite or calcium oxalate monohydrate. The fitted parameter $L\sigma^*/M_{50}$ takes on a value of 0.18 ± 0.02. The kinetics and associated model are capable of describing the evolving particle size distributions very well. Finally, a hypothesis is advanced to describe the aggregation of small inorganic crystals in supersaturated solutions. *AIChE J,* 50: 2772–2782, 2004
Keywords: Vaterite, calcium carbonate, crystal growth, aggregation, agglomeration

Introduction

Precipitation from aqueous solution is often determined by kinetic factors through the formation of thermodynamically metastable phases. The study of particle rate processes of such phases, such as crystal growth and aggregation, is complicated because of the inherent transformation toward more stable polymorphs. Kinetically stabilized phases are favored in systems of high and maintained supersaturation values, such as continuously operating crystallizers operating at the demand of high throughputs.

Among the barely soluble substances, calcium carbonate is the most studied system because the precipitation of calcium carbonate is a widely occurring process in nature as well as an important operation in industry (Tai and Chen, 1998). The unwanted precipitation of calcium carbonate is a problem in heat exchangers and it is one of the more important scale-forming minerals in oil and gas production. In the precipitation of calcium carbonate three crystalline polymorphs are known to form. They are, in order of increasing stability, Vaterite, aragonite, and calcite.

Vaterite acts as a precursor in the formation of calcite and/or

Correspondence concerning this article should be addressed to J.-P. Andreassen at jensp@chemeng.ntnu.no.

aragonite, often resulting in a mixture of polymorphs (Ogino et al., 1987), where the polymorphic abundance is controlled by the individual nucleation and growth rates. High yield production of calcium carbonate may give predominately Vaterite because of the sustained supersaturation values. Despite this, there are relatively few data available in the literature for the growth and aggregation of Vaterite. The crystal growth has been claimed to follow a parabolic rate law with rates that are ten times higher than those for calcite (Kralj et al., 1990). Other results, from mixed suspension–mixed product removal (MSMPR) studies, point to particle growth kinetics dominated by agglomeration (Hostomský and Jones, 1991). The cauliflower-like appearance of Vaterite particles often suggests the latter to be true, but microscopic evidence may be misleading in this context, and a more phenomenological approach is necessary to separate the contributions from crystal growth and aggregation. In a seeded-batch system, with negligible nucleation and particle breakage, crystal growth and aggregation will be the only phenomena that alter the amount of solid material present, or the particle size distribution. In such systems, crystal growth and aggregation rates can be extracted from experimentally measured particle-size distributions (PSDs) as a function of time, by the method developed by Bramley et al. (1996). By correlation with the supersaturation ratio, information about the mechanism of the two processes may also be obtained. The intention of this work is to investigate the growth and aggregation of Vaterite in seeded-batch experiments.

Theory

Supersaturation

The relative supersaturation σ is defined as $S - 1$, where the supersaturation ratio S for Vaterite is defined by

$$S = \left(\frac{IAP}{K_{SP}(\nu)} \right)^{1/2} \tag{1}$$

where $IAP = a_{Ca^{2+}} a_{CO_3^{2-}}$ is the ionic activity product and $K_{SP}(\nu)$ is the thermodynamic solubility product for Vaterite. Values of $K_{SP}(\nu)$, in the range between 0 and 90°C, are determined from the relationship reported by Plummer and Busenberg (1982), where T is given in K

$$\log K_{SP}(\nu) = -172.1295 - 0.077993T + 3074.688/T + 71.595 \log T \tag{2}$$

Changes in supersaturation can either be determined directly by activity measurements in the solution or indirectly through a mass balance, which takes into account the initial solution composition and the measured increase in particle volume obtained from changes in the PSD. The latter approach was successfully adopted by Bramley et al. (1996), for the determination of aggregation and growth rates in batch precipitation of calcium oxalate monohydrate.

In the present work, besides Ca^{2+} and CO_3^{2-} ions the solution also contains approximately 0.15 M $NaNO_3$ to facilitate the use of the Coulter Counter for particle size measurements. The presence of all these ions in water gives rise to the formation of other chemical species. Different equilibria as well as the ionic strength govern the activity of the different species. The important equilibria are given in Eqs. 3–9. Equilibrium constants (at 25°C) in Eqs. 3, 4, 7, and 8 are taken from Plummer and Busenberg (1982), in Eq. 6 from Kralj et al. (1990), and in Eqs. 5 and 9 from Collier and Hounslow (1999)

$$H^+ + OH^- \rightleftharpoons H_2O \qquad K_W = 9.954 \times 10^{13} \tag{3}$$

$$H^+ + CO_3^{2-} \rightleftharpoons HCO_3^- \qquad K_{HCO_3^-} = 2.132 \times 10^{10} \tag{4}$$

$$H^+ + HCO_3^- \rightleftharpoons H_2CO_3\,(aq) \qquad K_{H_2CO_3} = 2.246 \times 10^6 \tag{5}$$

$$Na^+ + CO_3^{2-} \rightleftharpoons NaCO_3^- \qquad K_{NaCO_3^-} = 18.62 \tag{6}$$

$$Ca^{2+} + CO_3^{2-} \rightleftharpoons CaCO_3\,(aq) \qquad K_{CaCO_3} = 1675 \tag{7}$$

$$Ca^{2+} + HCO_3^- \rightleftharpoons CaHCO_3^+ \qquad K_{CaHCO_3^+} = 12.76 \tag{8}$$

$$Ca^{2+} + OH^- \rightleftharpoons CaOH^+ \qquad K_{CaOH^+} = 25.12 \tag{9}$$

The above equilibria display how the concentrations of Ca^{2+} and CO_3^{2-} will be altered by the formation of ion complexes. To calculate the activity from the known concentrations, activity coefficients must be calculated. This is possible by the use of Davies' modification to the Debye–Hückel theory (Davies, 1962), which is given in the following equation

$$-\log(\gamma_{z_i,\pm}) = A z_i^2 \left(\frac{\sqrt{I}}{1 + \sqrt{I}} \right) + 0.3I \tag{10}$$

The activity coefficient γ depends on the charge z_i of the ions, the ionic strength I, and the Debye–Hückel constant A of the system. A has the value of 0.509 for this system at 25°C and values at other temperatures were determined by the relationship reported by Kralj et al. (1990).

The ionic strength I is dependent on the concentration of the ionic species c_i, according to the following equation

$$I = \frac{1}{2} \sum_i c_i z_i^2 \tag{11}$$

Because some of the equilibria involve a change in the number of ions present, an iterative procedure is required to solve the series of equations for the ion concentrations, activity coefficients, and the total ionic strength.

Growth

Electrolytes crystallizing from aqueous solution (Nielsen, 1984) may grow by widely different rate-determining mechanisms:

- transport (diffusion)/surface adsorption
- surface spiral growth
- surface nucleation (polynuclear growth)

Expressions for the growth rate as a function of the relative supersaturation ($S - 1$) give the linear, parabolic, and exponential rate law for these three cases, respectively:

$$G = k_1(S - 1) \tag{12}$$

$$G = k_2(S - 1)^2 \tag{13}$$

$$G = k_3 S^{7/6}(S - 1)^{2/3}(\ln S)^{1/6}\exp[-K/(\ln S)] \tag{14}$$

The overall linear growth rate G is defined as the rate of change of a typical dimension of a crystal or particle with time. Equivalent sphere diameter is a typical linear dimension and this is the value reported by the Coulter Multisizer. Half of this value, the rate of change of particle radius ($\dot{r}$) is frequently used, yielding, for a parabolic rate law

$$\dot{r} = k_r(S - 1)^2 \tag{15}$$

The growth rate of sparingly soluble salts is often found to be surface reaction controlled, quite often following the parabolic relationship of Eq. 13. Previous results for the growth of Vaterite in the literature have shown that the particles grow by a surface reaction–controlled mechanism characterized by a parabolic rate law. This research has resulted in quite different values for the growth rate constant k_r at 25°C, 1.06×10^{-10} and 1.17×10^{-10} m s^{-1} for $\sigma < 2.5$ at pH = 9.0 and 10.0, respectively (Spanos et al., 1998); 5.6×10^{-10} m s^{-1} for $\sigma < 2$ (Kralj et al., 1990); and 2.4×10^{-12} m s^{-1} for $\sigma < 1$ (Verdoes et al., 1992).

Aggregation

The aggregation rate constant may be described as a kernel $\beta(L, \lambda)$ (m^3·s^{-1}) that represents the rate constant for successful collisions between two particles of sizes L and λ. This kernel is assumed to be the product of two factors, $\beta(L, \lambda) = \beta_0 \times f(L, \lambda)$. β_0 is not dependent on the size of the colliding particles, but is a function of the operation conditions such as the solution composition and the fluid force acting on the newly collided particles. The size-dependent part of the kernel $f(L, \lambda)$ reflects the mechanism thought to have caused aggregation. Several results indicate that the aggregation process is well described by the size-independent kernel, β_0, alone [that is, $f(L, \lambda) = 1$]. Collier and Hounslow (1999) found that β_0 depends on the solution supersaturation by following the same dependency as the growth rate. The linear relationship between the success of particle collisions and the growth rate G points to an aggregation process controlled by the growth of a crystalline neck, which is able to withstand the periodic, disruptive hydrodynamic forces in the solution. An increase in the average fluid shear rate resulted in decreasing β_0 values by reducing the contact time between two colliding particles.

Based on a large collection of data for the precipitation of inorganic salts, Hounslow et al. (2001) developed an analysis that attempts to formulate general kinetic equations for the aggregation process based on a set of volume-averaged properties. They describe the aggregation rate as the product of the collision rate and an aggregation efficiency ψ. They show that the average efficiency for a vessel may be calculated from

$$\bar{\psi} = \frac{\bar{\beta}_0}{\bar{d}_{3.0}^3}\sqrt{\frac{15\nu}{8\pi\bar{\varepsilon}}} \tag{16}$$

They then relate this to the strength of the newly formed neck in a new aggregate compared to the disruptive hydrodynamic forces acting on it. Liew et al. (2003) modified this analysis to allow that the initial contact between two particles might be either a line or a point; they conclude that it is a line, and so the dimensionless strength M_1 may be calculated as follows

$$M_1(\bar{\varepsilon}) = \frac{L\sigma^* G}{\rho \bar{d}_{3.0}^2 \bar{\varepsilon}} \tag{17}$$

The apparent yield stress (σ^*) is a material property that combines the material strength, the geometry of the pore between the two particles, and the inclination of the touching surfaces; L is the length of the initial contact between two particles; G is the particle growth rate; ρ is the fluid density; $\bar{d}_{3.0}$ is the average particle diameter; ν is the kinematic viscosity; $\bar{\beta}$ is the volume-averaged aggregation rate constant; and $\bar{\varepsilon}$ is the time and volume average of the turbulent energy dissipation rate.

Analysis of data for calcite and calcium oxalate monohydrate (COM) have shown that the previously determined dependencies on stirrer speed and initial ionic ratios (Hounslow et al., 2001) disappear when moving from (β_0, G) space to [$\bar{\psi}$, $M(\bar{\varepsilon})$] space.

Liew et al. (2003) show that the relationship between efficiency and dimensionless strength can be described by a single parameter, M_{50}, the dimensionless strength corresponding to an efficiency of 0.5, so that

$$\psi = \frac{M_1/M_{50}}{1 + M_1/M_{50}} \tag{18}$$

Experimental

Seed preparation

The mixing of calcium- and carbonate-containing solutions usually results in a mixture of polymorphs. According to the literature it is difficult to obtain pure Vaterite, especially when the starting concentrations correspond to an ionic activity product (IAP) above the solubility product of amorphous calcium carbonate (ACC) (Ogino et al., 1987). If the starting IAP is between K_{SP}(ACC) and K_{SP}(Vaterite) the solution precipitates 100% Vaterite. This was confirmed by Kralj et al. (1990) in their study of unseeded growth of Vaterite. Spontaneous precipitation at this level of reactant concentrations, however, will produce a quite dilute system of small seed particles. A reproducible seed-preparation technique had to be developed that should fulfill the following requirements:

- It should produce close to pure Vaterite.
- The majority of the Vaterite particles should have a size larger than the lowest size channel of the Coulter Multisizer (~ 2 μm).
- The mass fraction of seeds in solution should be as high as possible, to give the smallest possible volume of mother liquor, to limit the dilution of the seeded system.
- The mother liquor should be depleted with respect to both

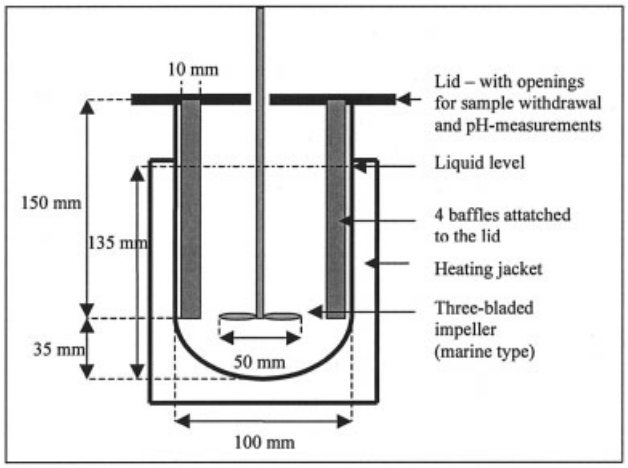

Figure 1. Jacketed glass crystallizer with four baffles and a stainless steel propeller-type stirrer.

calcium and carbonate ions, which implies that the initial concentrations of the two ions should be the same.

- The number and volume distributions of the seed material should be reproducible when constant volume withdrawals are made from the same seed batch.
- Transformation of the Vaterite particles cannot be accepted within a certain time interval if seed withdrawals are to be made from the same batch.

A method to produce seeds that fulfill the above criteria was found by trial and error. A 0.1 M calcium nitrate solution (250 mL) and a 0.1 M sodium carbonate solution (250 mL) were poured simultaneously (for 5 s) into a stirred vessel, as shown in Figure 1. The vessel was jacketed for temperature control, and stirred by a digital stirrer engine (IKA) equipped with a 50-mm three-bladed propeller-type impeller, operating at a constant stirrer rate of 1500 rpm. The same vessel was used for the seeded experiments and this equipment is identical to that used in the work by Collier and Hounslow (1999) on the growth and aggregation of calcite and COM, for easier comparison of results. All reagents were analytically pure, and distilled water was used throughout. The solutions were filtered through 0.22-μm membrane filters (Millipore, Milford, MA).

The density of the seed particles is expected to be lower than the theoretical value of 2690 kg m^{-3}, given that the particles are polycrystalline. The true density of the particles was determined by seeding a solution of zero relative supersaturation and determining the volume of these seed particles by repeated Multisizer measurements. The mass of particles in a corresponding sample was calculated and the density could then be determined.

Seeded-batch experiments

Supersaturated solutions of calcium carbonate were prepared by mixing equimolar solutions of calcium nitrate and sodium carbonate, both containing 0.15 M sodium nitrate for use of the Coulter Multisizer. The sodium carbonate solution was added to the calcium nitrate solution just before addition of 15 mL volume of seed solution. Immediately after the seeds were added, the first sample (sample volume 10 mL) was quickly withdrawn from the system by an automatic pipette positioned 5 cm below the liquid surface, transferred to a small beaker, and immediately analyzed by a Coulter Multisizer to determine the particle size distribution. The sampling frequency was limited to a maximum of 1/min by the experimental technique and the analysis time of the Multisizer. Samples were analyzed every minute for 20 min.

Some 35 experiments were performed in a semiordered fashion at 25°C to achieve information about how the system behaves at different conditions of supersaturation and stirring speed. The initial relative supersaturation was varied to obtain a wide range of growth rate values and to check for potential changes in the growth mechanism. Initial relative supersaturation (σ) values of 1.66, 2.08, 2.48, 4.00, and 6.70 were used, corresponding to initial reactant concentrations in the vessel of 0.00150, 0.00175, 0.00200, 0.00300, and 0.00500 M. A 2^3-experimental design was performed to evaluate the effect of temperature, ionic strength, and stirring speed. The temperature was varied between 25 and 40°C, stirring rate between 400 and 1200 rpm, and the ionic strength by adding sodium nitrate from the default concentration of 0.15 to 0.50 M. The initial concentration of reactants in the vessel was 0.0020 M. Two parallel experiments were performed for each set of the parameters. Several experiments were also conducted at 50°C.

Methods for calculation of growth and aggregation rates

The growth and aggregation rates may be derived independently from the change in particle numbers and volume, respectively, as follows

$$\frac{dm_0}{dt} = -\frac{1}{2}\,\beta_0 m_0^2 \tag{19}$$

$$\frac{dm_3}{dt} = 3Gm_2 \tag{20}$$

where m_i is the ith moment of the particle size distribution. In the case when seed particles grow into the field of view of the particle-size analyzer (expressed by the source function, B_u), or either growth or aggregation is size dependent, a differential form of the population balance must be used. Bramley et al. (1996) provide the following analysis.

The three unknown rate constants, β_0, G, and B_u, can be found from the following three equations

$$\dot{m}_0 = \beta_0\Phi_0 + B_u \tag{21}$$

$$\dot{m}_3 = G\Phi_3 + B_u\bar{L}_1^3 \tag{22}$$

$$\dot{N}_1 = G\Phi_2 + \beta_0\Phi_1 + B_u \tag{23}$$

where the values of $\dot{m}_1$, $\dot{m}_3$, $\dot{N}_1$, Φ_0, Φ_1, Φ_2, and Φ_3 can be calculated from the experimentally measured particle size distributions.

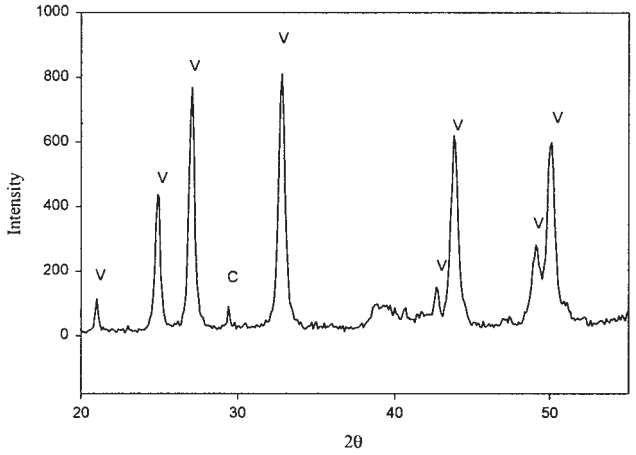

Figure 2. X-ray diffraction diagram for the seed population.

V, Vaterite; C, calcite.

Results and Discussion

Seed particles

The procedure described in the experimental section resulted in a system of IAP above that of K_{SP}(ACC). Despite the fact that ACC formed initially, it rapidly (within 5 min) transformed to produce close to 100% Vaterite, as evident by the X-ray diffraction diagram in Figure 2. This Vaterite population was stable for about 20 h before it transformed to calcite so that several seeded experiments could be performed based on the same seed population.

The relatively narrow size distribution shown in Figure 3 is a result of predominantly single spherical particles (spherulites) as shown at two different magnifications in Figure 4. The density of the particles was found to be 2020 kg·m^{-3} compared to the theoretical value of 2690 kg·m^{-3}. Seeding to a solution of zero relative supersaturation showed that the particle size distribution remained unchanged, even at high stirring speeds (up to 2000 rpm).

The seed fabrication technique satisfied the criteria of particle size, suspension density, and reproducibility listed in the experimental section. The invariance of the PSD in saturated solutions confirmed the activity calculations (no growth or dissolution) and also that breakage is negligible.

Growth rates

The growth rates were measured as a function of decreasing supersaturation in several experiments starting at different values of the saturation ratio. For experiments at 25°C, the results are shown in Figure 5. The best-fit line shown there corresponds to

$$G\ (\mathrm{ms}^{-1}) = (1.05 \pm 0.01) \times 10^{-9}(S-1)^2 \qquad (24)$$

The error quoted here, and in other estimates, is one standard deviation in the mean (that is, the standard error). The 95% confidence interval for the estimate of the parameter therefore extends over approximately twice the range indicated.

Because the Coulter Multisizer reports particle diameters, the growth rate G is a measure of the rate of particle diameter increase. Half of this value, the rate of change of the particle radius, $\dot{r} = dr/dt$ (m·s^{-1}), is frequently used and the overall growth rate can therefore be written as

$$\dot{r}\ (\mathrm{ms}^{-1}) = (0.527 \pm 0.006) \times 10^{-9}(S-1)^2 \qquad (25)$$

The value of $k_r = 0.527 \pm 0.006 \times 10^{-9}$ m·s^{-1} at 25°C compares well with the work by Kralj et al. (1990). They used a solution-based technique, where the growth rate is determined by calculating the reduction in Ca^{2+} and CO_3^{2-} activities. Growth for $\sigma < 2$ was investigated at temperatures between 10 and 45°C and at ionic strengths from 15 to 315 mM. The kinetics were parabolic and the growth rate constant varied from 0.180×10^{-9} m·s^{-1} at 11.4°C to 1.860×10^{-9} m·s^{-1} at 42.5°C, with a slight increase as a function of ionic strength. The results at 25°C were in the range from $k_r = 0.560 \times 10^{-9}$ m·s^{-1} to $k_r = 0.610 \times 10^{-9}$ m·s^{-1}, which all slightly exceed the value obtained in the present work. Kralj et al. (1990) base their approach on the assumption that the change in surface area is a function of growth only because they did not provide an analysis of aggregation and counted the particles only initially (under a light microscope). They did report the density of the particles, which most likely means that they based their calculations on the theoretical value. This should give a higher packing degree and therefore a lower growth rate compared to that of the present work, where the applied density is lower than the theoretical one. The solution-based technique provides more accurate growth rate values than the technique based on changes in the particle size distribution, but may nevertheless contain systematic deviations because of the above-mentioned assumptions. Nevertheless, the values of the present work and those presented by Kralj et al. (1990) agree reasonably well with those obtained by Verdoes et al. (1992) and Spanos et al. (1998). The former study included both seeded and unseeded experiments to obtain information about the kinetics and mechanism of nucleation and growth. The growth rate was found to be parabolic with respect to relative supersaturation, indicating a spiral growth mechanism and the growth rate constant was determined to 2.4×10^{-12} m·s^{-1} at 25°C for $\sigma < 1$. Verdoes

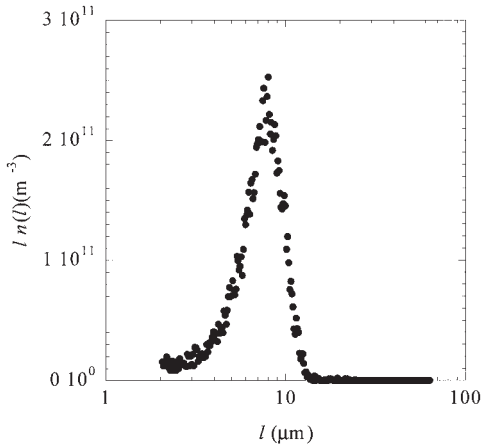

Figure 3. Size-distribution of Vaterite spherulites seeded to a solution of zero relative supersaturation.

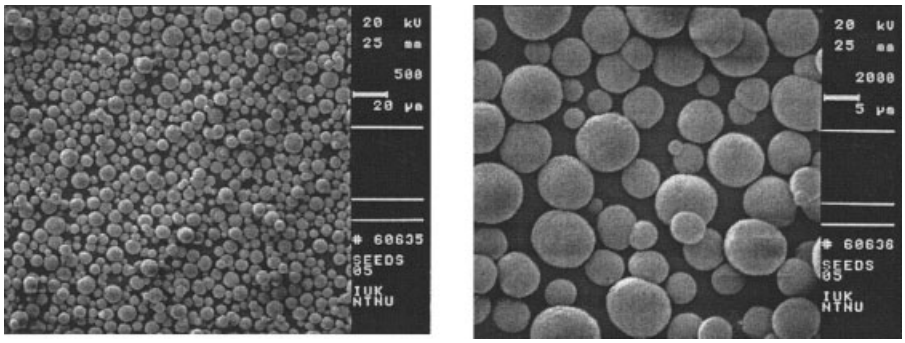

Figure 4. Micrographs of Vaterite seeds at two different magnifications.

Left: scale bar = 20 μm. Right: scale bar = 5 μm.

et al. (1992) compared this value to that of 5.6×10^{-10} m·s^{-1}, as reported by Kralj et al. (1990), and attributed the discrepancy to the effect of nonstoichiometry of their calcium and carbonate solutions. Spanos et al. (1998) investigated the kinetics of Vaterite precipitation in different constant supersaturation experiments, confirmed the parabolic dependency, and determined the growth rate constant to 1.06×10^{-10} and 1.17×10^{-10} m·s^{-1} for $\sigma < 2.5$ at pH = 9.0 and 10.0, respectively.

The results from the literature are recorded below $(S - 1) = 2.5$. The present study has shown that Vaterite grows by a parabolic rate law up to a value of $(S - 1) = 6$. Parabolic rate laws have previously been determined for several electrolytes (Nielsen and Toft, 1984) in the range of higher S-values ($S > 2$), where the requirements of the classical Burton–Cabrera–Frank (BCF) theory no longer are fulfilled, that is, that $(S - 1)\ln S \approx (S - 1)^2$. Nielsen and Christoffersen (1982) explained how this can be attributed to the fact that integration of building blocks into kinks is the controlling mechanism, rather than the adsorption at the steps of the spiral. The supersaturation dependency in the former case is $(S - 1)S^{1/2}\ln S$, which happens to be almost proportional to $(S - 1)^2$ in the range $1 < S < 30$ and this explains the validity of the parabolic rate law even for large supersaturations.

The result of the experiments performed at 40°C is shown in Figure 6. The corresponding growth rates are given in Eqs. 26 and 27. The growth rate constant at 40°C was determined to be $k_r = 1.98 \pm 0.08 \times 10^{-9}$ m·s^{-1}, which is about four times the value obtained at 25°C

$$G\ (\mathrm{ms}^{-1}) = (4.0 \pm 0.2) \times 10^{-9}(S - 1)^2 \tag{26}$$

$$\dot{r}\ (\mathrm{ms}^{-1}) = (1.98 \pm 0.08) \times 10^{-9}(S - 1)^2 \tag{27}$$

The relation between the growth rate constant k_r and the absolute temperature T is given by the Arrhenius equation

$$\frac{d \ln k_r}{dT} = \frac{E_a}{RT^2} \tag{28}$$

where E_a is the activation energy and R is the gas constant.

The high growth rate at elevated temperatures complicates the determination of the growth rate constant with the method applied in the present work. The depletion of calcium and carbonate ion activities is very rapid, resulting in few and uncertain data points. Attempts to produce data at 50°C were unsuccessful. With only two measurements of the growth rate constant (assuming that the activation energy is constant in the temperature interval), the following equation is obtained by integration of Eq. 28 between the limits T_1 and T_2

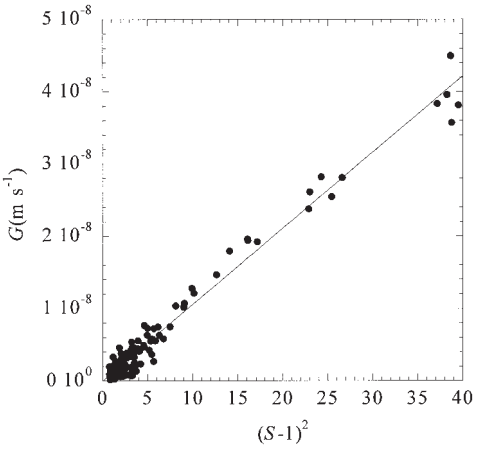

Figure 5. Growth rate G as a function of the relative supersaturation ($S - 1$), at 25°C.

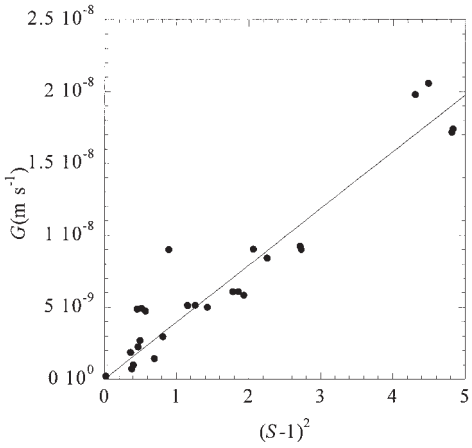

Figure 6. Growth rate G as a function of relative supersaturation ($S - 1$), at 40°C.

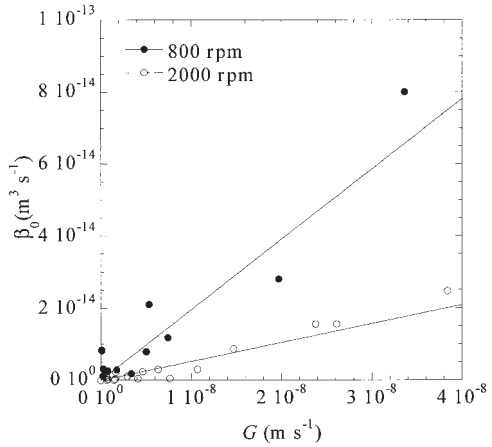

Figure 7. Relationship between the aggregation rate constant and the growth rate at two different stirrer speeds at 25°C.

$$E_a = \frac{RT_1T_2}{T_2 - T_1} \ln \frac{k_{r,2}}{k_{r,1}} \tag{29}$$

By insertion of the temperatures and growth rate constants, an activation energy value of 68 ± 3 kJ/mol is obtained, which compares with the value 57.1 kJ/mol determined by Kralj et al. (1990).

Aggregation rates

The extraction of the aggregation rate constant β_0 is based on the assumption of size-independent aggregation, which means that the rate constant of collisions is the same for all pairs of particles. A size-independent aggregation kernel has already been reported to give the best description of the aggregation of calcite (Collier and Hounslow, 1999), Vaterite (Wójcik and Jones, 1997), COM (Bramley et al., 1996), and gibbsite (Ilevski and Hounslow, 1995; Seyssiecq et al., 2000). The choice of this kernel will be confirmed once the kinetic data are extracted.

Figure 7 shows the relationship between the growth rate G and the aggregation rate constant β_0, at 25°C, for two different stirrer speeds at the same initial reactant concentration of 0.00500 M ($\sigma = 6.7$). This linear relationship reflects that the success of aggregation is directly dependent on the rate at which a bridge forms between two colliding particles (that is, the growth rate). The ratio β_0/G is plotted in Figure 8 for all the experiments reported here. The ratio decreases with increased stirrer speed, which is in accordance with the results presented for calcite and COM by Collier and Hounslow (1999). Experiments performed at a stirrer speed of 200 rpm failed to produce representative samples and the third moment decreased with time, probably as a result of particle sedimentation in the vessel.

Micrographs of resulting particles after 20 min are shown in Figure 9 for stirring rates of 400 and 2000 rpm at the same initial supersaturation values. The former case resulted in larger aggregated particles, typically consisting of three to six primary Vaterite spheres, whereas the intensive stirring at 2000 rpm results in a product similar to the starting seed population (Figure 3) with an approximate doubling of the primary sphere size and the formation of some doublets.

Recent investigations of the effect of growth rate and stirrer speed on aggregation in precipitation processes are available in the literature (Mumtaz and Hounslow, 2000; Seyssiecq et al., 2000; Zauner and Jones, 2000), resulting in somewhat deviating opinions about the basic principles of the aggregation process. Two particles come together as a result of the orthokinetic collision frequency but the success of aggregation is dependent on growth-controlled cementation. The growth of a sufficiently strong bridge between the particles during the time of contact is necessary to prevent breakup of the two particles as a consequence of high shear rates in the solution. The treatments differ in whether the disintegration of an aggregate of two barely attached particles should be considered as an unsuccessful aggregation event or as a breakage event. The latter approach should result in higher aggregation rates to produce a PSD that is consistent with that of the former approach.

The aggregation rates published by Wójcik and Jones (1997) are substantially lower (by a factor of 10) than the values presented in the present work, despite the fact that they included breakage in their analysis. Their results also showed the opposite dependency of stirrer speed compared to those presented here.

Collier and Hounslow (1999), Hounslow et al. (1999), and Mumtaz and Hounslow (2000) found that the disruption rate was negligible and that breakup of newly formed doublets should be regarded as the result of reduced aggregation efficiency rather than breakage events. The aggregation rate is a product of this efficiency as well as the collision rate. An increase in the fluid shear rate enhances the collision rate. However, higher fluid shear rates also result in larger hydrodynamic forces and shorter timescales for bridge formation. As a consequence of the two opposing effects of the fluid shear rate on aggregation, a maximum in the aggregation rate constant as a function of fluid shear rate is expected. The results in Figure 8 reflect the situation of high collision rate and reduced aggregation efficiency. Both Mumtaz and Hounslow (2000) and Zauner and Jones (2000) produced aggregation data in the region of lower energy dissipation rates, confirming the above hypothesis by identifying a maximum in the aggregation rate

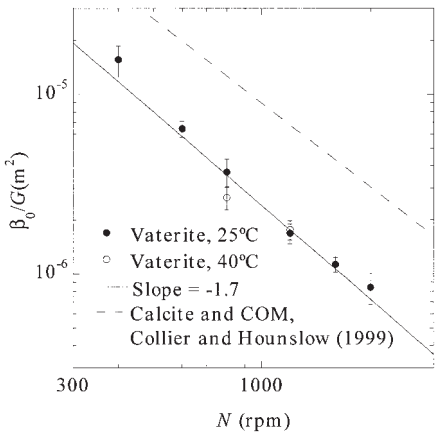

Figure 8. Effect of stirrer speed *N* on the ratio of aggregation and growth rates.

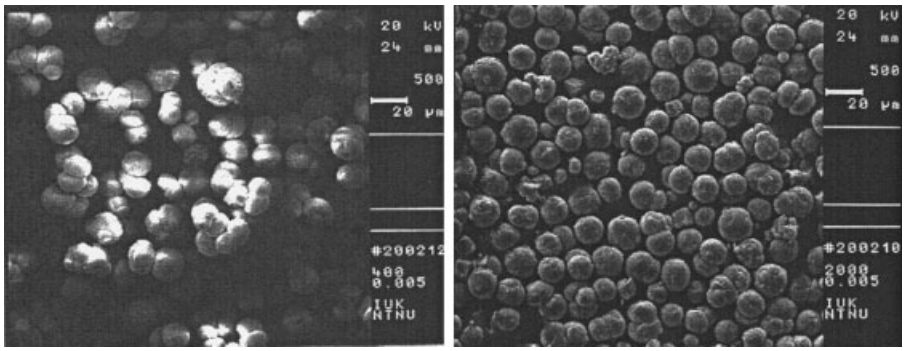

Figure 9. Vaterite seeds grown at high initial supersaturation (σ = 6.7) and stirred at 400 rpm (left) and 2000 rpm (right).

constant. This implies that the results in Figure 8 are obtained from experiments conducted at shear rates in excess of those corresponding to the maximum rate of aggregation.

Collier and Hounslow (1999) found that the slope of aggregation rate vs. growth rate was proportional to the stirrer speed to the power -1.5 for both calcite and COM. This result and the corresponding fit for Vaterite at 25 and 40°C are also shown in Figure 8. For Vaterite we find $\beta_0 \propto N^{-1.7\pm0.1}$.

The average shear rate, $\bar{\dot{\gamma}}$ (s^{-1}) in a stirred vessel is given by Koh et al. (1987)

$$\bar{\dot{\gamma}} = \sqrt{\frac{P}{\mu V}} = \sqrt{\frac{\bar{\varepsilon}}{\nu}} \tag{30}$$

where P (W) is the total power input ρ ($kg \cdot m^{-3}$) is the fluid density. It follows that P is proportional to the cube of the stirrer speed N (s^{-1}), given that the power number N_P at higher stirrer Reynolds numbers is expected to be constant

$$N_P = \frac{P}{\rho N^3 D^5} \tag{31}$$

Here D (m) is the diameter of the stirrer. A combination of Eqs. 30 and 31 reveals that the average shear rate is proportional to the stirrer speed to the power 1.5. This means that the dependency of stirrer speed on aggregation rate found for calcite and COM corresponds to aggregation rates that are inversely proportional to the average shear rate in the vessel. As will be seen later, if the aggregation rate is determined by the aggregation efficiency, which in turn depends on the dimensionless strength, it follows that if $\beta_0 \propto G$ then, necessarily, $\beta_0 \propto \bar{\varepsilon}^{-0.5} \propto \bar{\dot{\gamma}}^{-1} \propto N^{-1.5}$.

Although the slope of -1.7 ± 0.1 for the aggregation of Vaterite spherulites is quite close to the value obtained for calcite and COM (and the deviation can readily be explained by the effect of particle size), the magnitude of the aggregation to growth ratio differs substantially. Because the experimental equipment is comparable in both studies, an explanation to the lower aggregation efficiency of Vaterite should be sought in properties such as aggregate geometry and the yield stress, that is, the apparent yield stress parameter σ^* in Eq. 17.

The results at 40°C and stirrer speeds 800 and 1200 rpm, also displayed in Figure 8, show how the ratio β_0/G is comparable to the values obtained at 25°C, although both the growth and the aggregation rate increase with temperature. This result supports the proposed mechanism of deposition–cementation-controlled aggregation and shows that the apparent effect of temperature on aggregation rates stems entirely from the effect of temperature on growth rates.

Increasing the ionic strength had no significant effect on the aggregation rates (or the growth rates), although more experiments should be performed to reduce the error estimates to determine any potential effects. It is likely that the ionic strength already present in the standard experiments (≈0.17 M) is sufficient to cause a breakdown of the electric double layer and that the effect of increasing the concentration further is minimal. The effect of ionic strength (double layer) is not incorporated in the collision and aggregation efficiency model of Mumtaz et al. (1997), but it might be that particles will repel each other at lower ionic concentration thereby reducing both the aggregation and collision efficiency.

The growth and aggregation data for Vaterite are transformed to $[\bar{\psi}, M_1(\bar{\varepsilon})]$ space by Eqs. 16 and 17. The unknown strength parameter ($L\sigma^*$) is initially taken to be 0.722 N m^{-1}, as used by Liew et al. (2003). Figure 10 displays these data in two forms. The cloud of small points is the data for each of the sample times in each of the experiments. Data of this kind are inevitably scattered because they are deduced from numerical

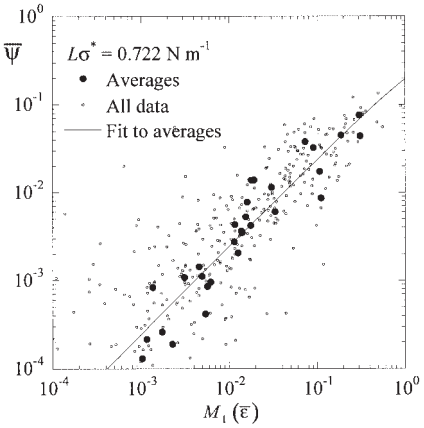

Figure 10. Aggregation efficiency as a function of dimensionless strength for Vaterite.

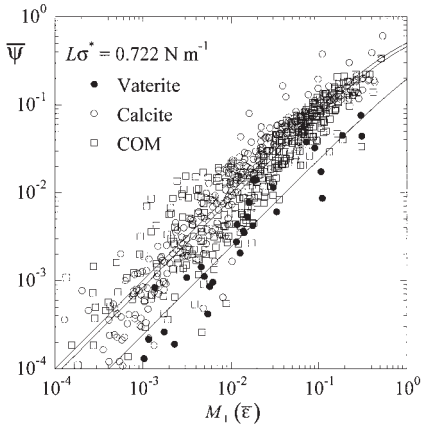

Figure 11. Aggregation efficiency as a function of dimensionless strength for Vaterite (present study), calcite, and COM (Liew et al., 2003).

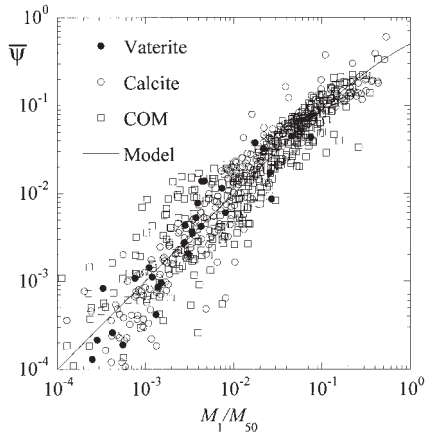

Figure 12. Aggregation efficiency as a function of dimensionless strength for Vaterite (present study), calcite, and COM (Liew et al., 2003) using the values of $L\sigma^*/M_{50}$ shown in Table 1.

estimates of the rates of change on the left-hand sides of Eqs. 21 to 23 and, as time proceeds in each experiment, these changes decrease in magnitude. However, because we expect that ψ is directly proportional to M_1 over much of each experiment, it follows that data averaged for each experiment (that is, over the sample times) will display the same relationship and the underlying data points. The data represented by the large markers in Figure 10 were obtained this way.

Figure 10 shows that when the dimensionless strength is low the efficiency is low and when one is high, so too is the other. In principle, if M_1 takes on a sufficiently large value ψ should become constant at a value near 1. In this study, however, such high values were not obtained and ψ is directly proportional to M_1 over the whole range of data.

It was remarked above that, if the aggregation rate constant is directly proportional to the growth rate, then according to the theory presented here, it must inevitably vary as the stirrer speed N, to a power of $-3/2$: if $\psi \propto G$ then $\psi \propto M_1$; thus, because $\beta_0 \propto \psi \bar{d}_{3,0} \bar{\varepsilon}^{0.5}$ and $\bar{\varepsilon} \propto N^3$, then

$$\beta_0 \propto \bar{d}_{3,0} G N^{-1.5} \tag{32}$$

In Figure 11 efficiency data for the present study are compared with those of Calcite and COM reported by Liew et al. (2003). It is clear that the Vaterite data show a similar dependency but are displaced to the right, or down. In other words, under the same conditions Vaterite shows significantly lower efficiencies than those of the other two systems.

Also shown in Figures 10 and 11 are curve fits, of the form of Eq. 18, from which it is possible to deduce a value for the ratio of parameters $L\sigma^*/M_{50}$. The fitted values are shown in Table 1.

Table 1. Parameter Values Used to Fit Eq. 18 to the Data in Figures 10 and 11

	Liew et al. (2003)		Present Work
	COM	Calcite	Vaterite
$L\sigma^*/M_{50}$ (N m^{-1})	0.61 ± 0.02	0.72 ± 0.03	0.18 ± 0.02

For each of the studies reported in Table 1, we expect M_{50} to have the same value (of about 1) because it depends only on the shape of the energy dissipation distribution, which in turn depends only on the Reynolds number (weakly) and the vessel geometry, and each was conducted in a vessel of the same geometry. It follows that Vaterite either has a much lower value of strength or the contact geometry is different. A smaller value of the apparent strength might well be the result of both different pore geometry and material strength. The spherical shape of Vaterite results in both wider pores and a smaller contact area than that of encounters between faceted particles. The strength of Vaterite may also be lower because it in fact grows as a polycrystalline particle of radiating crystallites. Similarly, the length of contact between two rough spherical particles might well be less than that between two nearly planar facets.

The parameters reported in Table 1 can now be used to correct the false assumption implicit in Figure 11 that $L\sigma^* = 0.722$ N m^{-1} in all cases; however, we must scale M_1 by M_{50} because we cannot make an independent measurement of its value. Figure 12 shows these results. We see that all three systems have superimposable behavior. We conclude that all three systems are governed by the same phenomena and that the model inherent in Eqs. 16 and 17 captures the essential character of those phenomena.

Size distributions

The growth and aggregation data reported above are deduced essentially from the measured rates of change of the total particles numbers and volume. In addition to these data we have measured the whole size distribution of each sample. We used the package *DPB* (Hounslow, 2003) to test the capacity of the deduced kinetics to predict the measured size distributions. For each experiment we take the initial measured distribution, and the kinetics reported above (that is, Eq. 24 and $L\sigma^*/M_{50} = 0.18$), and predict the evolving distribution. A typical set of results is shown in Figure 13. Clearly the measured and predicted data are in excellent agreement. That this should be the case for all the experiments reported here is confirmation that

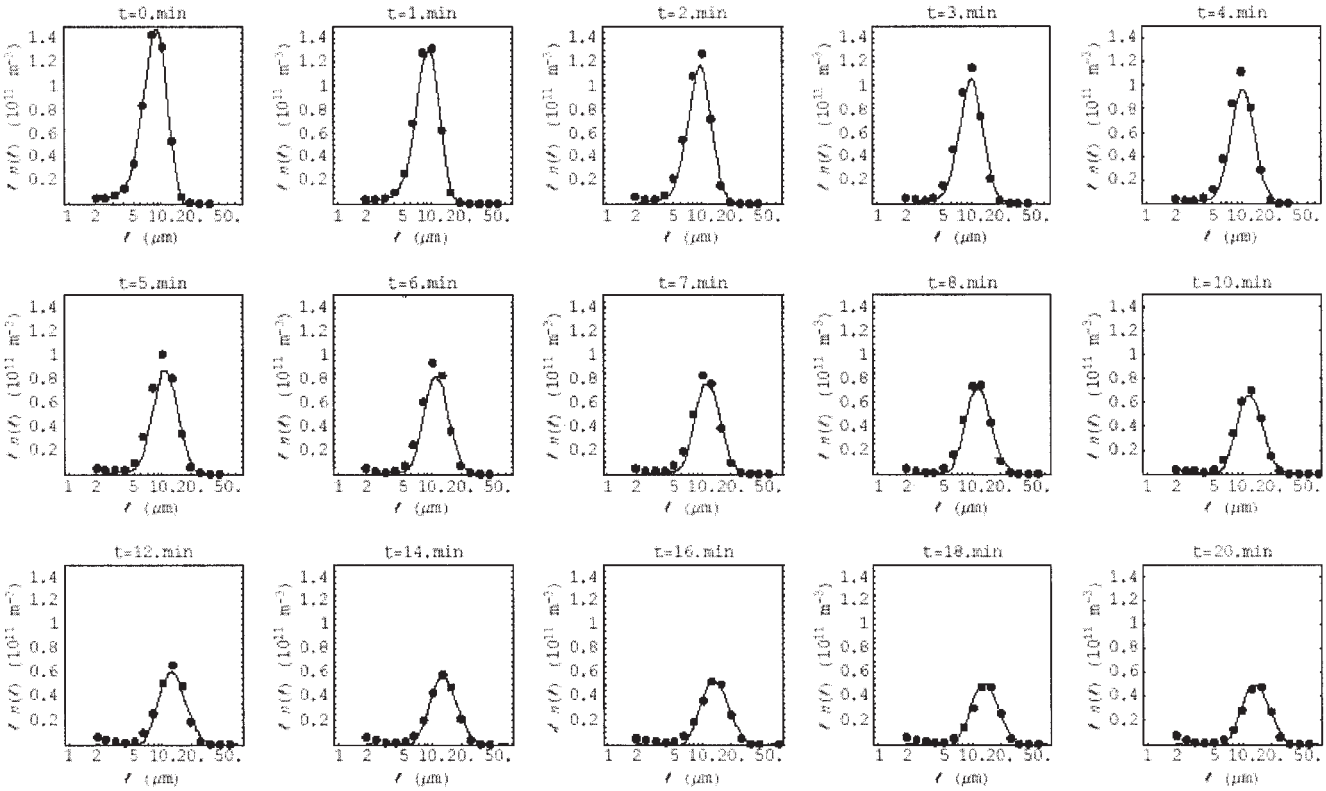

Figure 13. Typical predicted (lines) and measured (markers) number density functions showing an evolving PSD.

they can be described by *size-independent* crystal growth and an averaged *size-independent* aggregation rate constant.

Conclusions

A method to produce Vaterite seeds has been developed and the seeded-batch precipitation of Vaterite has been investigated to measure the growth and aggregation rates.

The growth of Vaterite spherulites was found to be size independent and second order in supersaturation with a growth rate constant of $k_r = 0.527 \pm 0.006 \times 10^{-9}$ m·s^{-1} at 25°C and $k_r = 1.98 \pm 0.08 \times 10^{-9}$ m·s^{-1} at 40°C, resulting in an activation energy of 68 ± 3 kJ/mol.

Aggregation of Vaterite spherulites was found to be size independent and the aggregation rate constant β_0 was linear in the instantaneous growth rate.

The ratio of β_0 to G was the same at 25 and 40°C, indicating that the success of an aggregation event depends on the growth of a crystalline bridge between two colliding particles. Aggregation decreases with increased stirrer speed, attributed to larger hydrodynamic forces acting on the colliding particles, and the reduced time of contact.

The ratio of β_0 to G was close to inversely proportional to the volume-averaged shear rate and the growth and aggregation behavior of Vaterite is comparable to that found for calcite and calcium oxalate monohydrate.

The three systems differ mainly by the value of the apparent yield stress, which is a conjunction of strength and shape parameters. The smaller aggregation efficiency found in the aggregation of Vaterite spherulites could be a result of the geometry of the contact point and/or a lower strength in the crystalline bridge that consolidates the aggregates.

The success of our approach in describing three different systems leads us to offer the following hypothesis:

For systems such as those reported here, that is,

- inorganic crystals growing in a supersaturated solution
- of size smaller than the Kolomogorov scale, but large enough to be subject to shear-induced aggregation
- in a turbulent, agitated vessel
- under conditions of elevated ionic strength

The rate of aggregation depends on

- the product of the rate of collisions and the aggregation frequency
- the collision frequency can be calculated satisfactorily from Smoluchowski's shear kernel based on average particle size

The aggregation efficiency depends only on

- the dimensionless strength M_1, defined in Eq. 17
- the nature of the flow field in the vessel

The dimensionless strength depends on

- the growth rate of the particles (G)
- the yield strength and contact geometry of the particles ($L\sigma^*$)
- the density of the solution (ρ)
- the average size of the particles ($\bar{d}_{3,0}$)
- the average rate of energy dissipation in the vessel ($\bar{\varepsilon}$)

The nature of the flow field determines

- the value of the average rate of energy dissipation in the vessel ($\bar{\varepsilon}$)

- the value of the dimensionless strength at which $\psi = 0.5$ (that is, M_{50})
- the nature of the relationship between ψ and M_1, such as $\psi \propto M_1$ or $\psi = (M_1/M_{50})/[1 + (M_1/M_{50})]$

Acknowledgments

This work was supported by The Norwegian Research Council, Norsk Hydro, Elkem, Norzink, Falconbridge and the EPSRC of the United Kingdom.

Notation

a = solute activity, mol L^{-1}
A = Debye–Hückel constant (in Eq. 10)
B_u = source function, $m^{-3}\cdot s^{-1}$
c_i = solute concentration
$\bar{d}_{3,0}$ = 3.0 mean particle size, m
D = stirrer diameter
E_a = activation energy
G = growth rate, $m\cdot s^{-1}$
k = growth rate constant, $m\cdot s^{-1}$
K_{SP} = solubility product
l = particle size, m
$\bar{L}_1$ = average particle size in the first size interval, m
I = ionic strength, $mol\cdot L^{-1}$
m_j = jth moment, $m^j\cdot m^{-3}$
$\dot{m}_j$ = rate of change of the jth moment, $m^j\cdot m^{-3}\cdot s^{-1}$
M = dimensionless strength of an aggregate
$M(\bar{\varepsilon})$ = M calculated from the average energy dissipation rate
M_{50} = dimensionless strength corresponding to an efficiency of 0.5
N = stirrer speed, min^{-1}
$\dot{N}_i$ = rate of change of particle number in the first size interval, $m^3\cdot s^{-1}$
N_P = power number of impeller
P = power input, W
S = supersaturation ratio
V = vessel volume
z_i = charge of ion

Greek letters

β = aggregation kernel, $m^3\cdot s^{-1}$
β = size-independent part of the aggregation kernel, $m^3\cdot s^{-1}$
ε = energy dissipation rate, $J\cdot kg^{-1}$
$\gamma_{\pm}$ = activity coefficient
$\dot{\gamma}$ = shear rate, s^{-1}
λ = parameter in logistic curve
ψ = aggregation efficiency
μ = dynamic viscosity, $Pa\cdot s^{-1}$
ν = kinematic viscosity, $m^2\cdot s^{-1}$
ρ = liquid density, $kg\cdot m^{-3}$
σ = relative supersaturation
σ^* = apparent yield strength, Pa

Acronyms

ACC = amorphous calcium carbonate
COM = calcium oxalate monohydrate
IAP = ionic activity product
MSMPR = mixed suspension–mixed product removal
SEM = scanning electron microscope
PSD = particle size distribution

Literature Cited

Bramley, A. S., M. J. Hounslow, and R. L. Ryall, "Aggregation during Precipitation from Solution. A Method for Extracting Rates from Experimental Data," *J. Colloid Interface Sci.*, **183**(1), 155 (1996).

Collier, A. P., and M. J. Hounslow, "Growth and Aggregation Rates for Calcite and Calcium Oxalate Monohydrate," *AIChE J.*, **45**(11), 2298 (1999).

Davies, C. W., *Ion Association*, Butterworth, Washington, DC (1962).

Hostomský, J., and A. G. Jones, "Calcium Carbonate Crystallization Kinetics, Agglomeration and Form during Continuous Precipitation from Solution," *J. Phys. D.*, **24**, 165 (1991).

Hounslow, M. J., *DPB*, www.shef.ac.uk/~ppg/dpb.htm (2003).

Hounslow, M. J., H. S. Mumtaz, A. P. Collier, J. P. Barrick, and A. S. Bramley, "Aggregation during precipitation—Putting the Pieces of the Puzzle Together," Proc. of the 14th Symp. on Industrial Crystallization (1999).

Hounslow, M. J., H. S. Mumtaz, A. P. Collier, J. P. Barrick, and A. S. Bramley, "A Micro-Mechanical Model for the Rate of Aggregation during Precipitation from Solution," *Chem. Eng. Sci.*, **56**, 2543 (2001).

Ilevski, D., and M. J. Hounslow, "Agglomeration during Precipitation: II. Mechanism Deduction from Tracer Data," *AIChE J.*, **41**, 525 (1995).

Koh, P. T. L., J. R. G. Andrews, and P. H. T. Uhlherr, "Modelling Shear-Flocculation by Population Balances," *Chem. Eng. Sci.*, **42**(2), 353 (1987).

Kralj, D., L. Bre[caron]cević, and A. E. Nielsen, "Vaterite Growth and Dissolution in Aqueous Solution—I. Kinetics of Crystal Growth," *J. Crystal Growth*, **104**, 793 (1990).

Liew, T. L., J. P. Barrick, and M. J. Hounslow, "A Micro-Mechanical Model for the Rate of Aggregation during Precipitation from Solution," *Chem. Eng. Technol.*, **26**(3), 282 (2003).

Mumtaz, H. S., and M. J. Hounslow, "Aggregation during Precipitation from Solution: An Experimental Investigation Using Poiseuille Flow," *Chem. Eng. Sci.*, **55**, 5671 (2000).

Mumtaz, H. S., M. J. Hounslow, N. A. Seaton, and W. R. Paterson, "Orthokinetic Aggregation during Precipiation: A Computational Model for Calcium Oxalate Monohydrate," *Trans. IChemE*, **75**(A), 152 (1997).

Nielsen, A. E., "Electrolyte Crystal Growth Mechanisms," *J. Crystal Growth*, **67**, 289 (1984).

Nielsen, A. E., and J. Christoffersen, "The Mechanisms of Crystal Growth and Dissolution," *Biological Mineralization and Demineralization*, G. H. Nancollas, ed., Springer-Verlag, Berlin, pp. 37–77 (1982).

Nielsen, A. E., and J. M. Toft, "Electrolyte Crystal Growth Kinetics," *J. Crystal Growth*, **67**, 278 (1984).

Ogino, T., T. Suzuki, and K. Sawada, "The Formation and Transformation Mechanism of Calcium Carbonate in Water," *Geochim. Cosmochim. Acta*, **51**, 2757 (1987).

Plummer, L. N., and E. Busenberg, "The Solubilities of Calcite, Aragonite and Vaterite in CO_2–H_2O Solutions between 0 and 90°C, and an Evaluation of the Aqueous Model for the System $CaCO_3$–CO_2–H_2O," *Geochim. Cosmochim. Acta*, **46**, 1011 (1982).

Seyssiecq, I., S. Veesler, D. Mangin, J. P. Klein, and R. Boistelle, "Modelling Gibbsite Agglomeration in a Constant Supersaturation Crystallizer," *Chem. Eng. Sci.*, **55**, 5565 (2000).

Spanos, N., and P. G. Koutsoukos, "Kinetics of Precipitation of Calcium Carbonate in Alkaline pH at Constant Supersaturation. Spontaneous and Seeded Growth," *J. Phys. Chem. B*, **102**, 6679 (1998).

Tai, C. Y., and F.-B. Chen, "Polymorphism of $CaCO_3$ Precipitated in a Constant-Composition Environment," *AIChE J.*, **44**(8), 1790 (1998).

Verdoes, D., D. Kashchiev, and G. M. van Rosmalen, "Determination of Nucleation and Growth Rates from Induction Times in Seeded and Unseeded Precipitation of Calcium Carbonate," *J. Crystal Growth*, **104**, 793 (1992).

Wójcik, J. A., and A. G. Jones, "Experimental Investigation into Dynamics and Stability of Continuous MSMPR Agglomerative Precipitation of $CaCO_3$ Crystals," *Trans. IChemE*, **75**(A), 113 (1997).

Zauner, R., and A. G. Jones, "Determination of Nucleation, Growth, Agglomeration and Disruption Kinetics from Experimental Precipitation Data: The Calcium Oxalate System," *Chem. Eng. Sci.*, **55**, 4219 (2000).

Manuscript received Dec. 22, 2003, and revision received Feb. 18, 2004.